

# *In Vivo* SELEX of an Inhibitory NSCLC-Specific RNA Aptamer from PEGylated RNA Library

Hanlu Wang,<sup>1</sup> Yibang Zhang,<sup>2,3</sup> Haiping Yang,<sup>2</sup> Meng Qin,<sup>1,2</sup> Xinxin Ding,<sup>1,4</sup> Rihe Liu,<sup>1,5</sup> and Yongping Jiang<sup>1,2</sup>

<sup>1</sup>Biopharmaceutical R&D Center, Chinese Academy of Medical Sciences & Peking Union Medical College, Suzhou, Jiangsu 215126, China; <sup>2</sup>Biopharmagen Corp., Suzhou, Jiangsu 215126, China; <sup>3</sup>Department of Pharmaceutics, School of Pharmacy, Jiangsu University, Zhenjiang, Jiangsu 212013, China; <sup>4</sup>Department of Pharmacology and Toxicology, College of Pharmacy, University of Arizona, Tucson, AZ 85721-0207, USA; <sup>5</sup>Division of Chemical Biology and Medicinal Chemistry, Eshelman School of Pharmacy and Carolina Center for Genome Sciences, University of North Carolina, Chapel Hill, NC 27599-7363, USA

**Aptamers are widely used in numerous biochemical, bio-analytical, and biological studies. Most aptamers are developed through an *in vitro* selection process called SELEX against either purified targets or living cells expressing targets of interest. We report here an *in vivo* SELEX in mice using a PEGylated RNA library for the identification of a 2'-F RNA aptamer (RA16) that specifically binds to NCI-H460 non-small-cell lung cancer cells with an affinity ( $K_D$ ) of  $9 \pm 2$  nM. Interestingly, RA16 potently inhibited cancer cell proliferation in a dose-dependent manner with an  $IC_{50}$  of 116.7 nM. When tested *in vivo* in xenografted mice, RA16 showed gradual migration toward tumor and accumulation at tumor site over time. An *in vivo* anti-cancer study showed that the average inhibition rate for mouse tumors in the RA16-treated group was  $54.26\% \pm 5.87\%$  on day 16 versus the control group. The aptamer RA16 adducted with epirubicin (RA16-epirubicin) showed significantly higher toxicity against targeted NCI-H460 cells and low toxicity against non-targeted tumor cells. Furthermore, RA16-epirubicin adduct exhibited *in vivo* anti-cancer efficacy, with an inhibition rate of  $64.38\% \pm 7.92\%$  when administrated in H460 xenograft mouse model. In summary, a specific bi-functional RNA aptamer RA16 was selected targeting and inhibiting toward NCI-H460 *in vitro* and *in vivo*.**

## INTRODUCTION

Lung cancer is the most common cause of cancer death all over the world. Non-small-cell lung cancer (NSCLC) accounts for 85%–90% of the lung cancer cases.<sup>1,2</sup> Conventional cancer therapies such as chemotherapeutics and radiation exhibit severe side-effects, including gastrointestinal distress, organ damage, and low-quality life.<sup>3,4</sup> New therapies including those based on monoclonal antibodies and their combination with other approaches have gained momentum as targeted therapeutics.<sup>4,5</sup> Over the past decades, great efforts have been made for the development of new targeted therapeutics to overcome the drawbacks associating with conventional therapies, among which epidermal growth factor receptor (EGFR) tyrosine kinase inhibitors (TKIs) are most commonly used for lung cancer treatment.<sup>6</sup> These are used in advanced NSCLC patients harboring EGFR mutations and have greatly enhanced survival rate by decreasing the toxicity as compared with cytotoxic chemotherapy. Nevertheless, resistance

invariably occurs,<sup>4,6,7</sup> highlighting the need to explore other strategies for targeting therapy. Moreover, tumor-specific biomarkers for NSCLCs are rare. Most reported biomarkers are not only expressed on tumor cells but also on normal cells, thereby restricting their clinical applications. Thus, identification of novel biomarkers for NSCLC diagnosis and development of more effective targeted therapeutics are of great importance.

Aptamers are single-stranded nucleic acids well-folded into diverse structures to bind specific targets. Since their first use in the 1990s,<sup>8,9</sup> many high-affinity aptamers that target small molecules to large proteins have been identified.<sup>10–13</sup> In comparison to antibodies, aptamers display obvious advantages such as easy chemical synthesis, none or low immunogenicity, smaller molecular size, and efficient entry into biological compartments.<sup>14</sup> Aptamers have been employed as drug carriers to deliver chemotherapeutics, small interfering RNAs (siRNAs), or nanoparticles into targeted tissues.<sup>13,15–18</sup> Thus, aptamers may serve as targeting ligands to direct therapeutics to the tumor site for increasing the effective concentration of drugs while minimizing the side effects to non-targeted normal tissues.

Systematic evolution of ligands by exponential enrichment (SELEX) and cell-SELEX are the major methods employed for aptamer selection. After several rounds of selection, enriched sequences emerge as the candidates binding their targets. Further identification and characterization of these candidate sequences result in their application for diagnosis or targeted therapy. The recombinant proteins or cells utilized for SELEX may not mimic the necessary antigen state or folding *in vivo*, owing to varying antigen density, interaction, and microenvironment. As a result, some aptamers selected using

Received 21 May 2017; accepted 6 December 2017;  
<https://doi.org/10.1016/j.omtn.2017.12.003>

**Correspondence:** Yongping Jiang, Biopharmaceutical R&D Center, Chinese Academy of Medical Sciences & Peking Union Medical College, 277 Qingqiu Street, Suzhou 215126, China.  
**E-mail:** [yjiang@biopharmagen.com](mailto:yjiang@biopharmagen.com)

**Correspondence:** Rihe Liu, Biopharmaceutical R&D Center, Chinese Academy of Medical Sciences & Peking Union Medical College, 277 Qingqiu Street, Suzhou 215126, China.  
**E-mail:** [rliu@email.unc.edu](mailto:rliu@email.unc.edu)



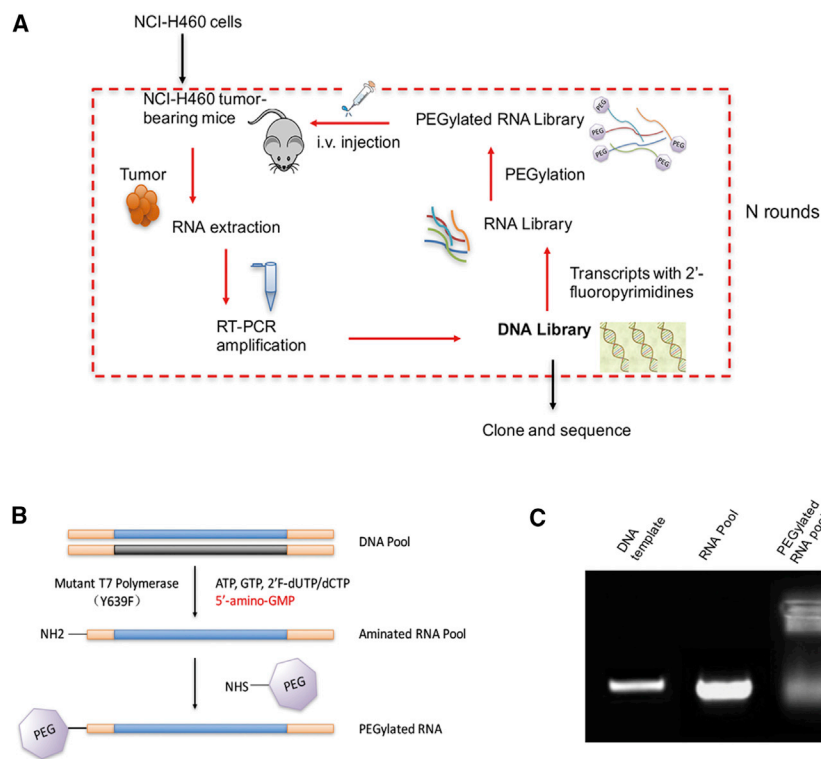


**Figure 1. *In vivo* SELEX Strategy**

(A) Workflow of the *in vivo* SELEX screening. The *in vitro* transcribed and PEGylated RNA pools were injected into the NCI-H460 tumor-bearing mice. Tumors were harvested, and RNAs trapped in the tumor were isolated and subjected to RT-PCR and *in vitro* transcription. After every three rounds of selection, the recovered DNA pool was cloned and sequenced for further analysis. (B) Schematic of PEGylation of aminated RNAs with NHS-PEG. (C) Analysis of RNA PEGylation on 3% agarose gel.

were incorporated during transcription using 2'-F-dCTP/dUTP, and 5'-PEGylation was performed in the entire selection process.<sup>22</sup> The recovered RNA sequences were reversely transcribed, and the resulting complementary DNAs (cDNAs) were PCR amplified for the next round of selection or cloned and sequenced after every three rounds of selection to monitor the *in vivo* SELEX progress (Figures 1A and 1B). As illustrated in Figure 1C, nearly 60%~70% of the RNAs were PEGylated with a shift band, ensuring the high diversity of the PEGylated RNA pool used in the selection. Following round 8, one RNA sequence (RA16) was identified as the most abundant sequence at a frequency of 21.2% by Sanger sequencing (Table 1).

The secondary structure of RA16 was predicted by Mfold<sup>23</sup> (version 3.1; online, <http://unafold.rna.albany.edu>). After several continuous selection rounds, RA16 dominated the pool by up to 94.7% (round 11) (Table 1), suggesting it is an aptamer that specifically binds to NCI-H460 tumor.

### Specificity and Affinity of the Selected RNA Aptamer RA16 *In Vitro*

We performed several experiments to confirm the specificity of the best sequence (RA16) against NSCLC. NCI-H460 cells used for establishing the tumor model were employed for the target-binding studies *in vitro*.<sup>24–26</sup> NCI-H460 cells incubated with Cy3-labeled RA16 showed strong fluorescent signal, indicating the specific binding between RA16 and NCI-H460 cells *in vitro*, whereas the negative control (initial RNA library) showed no detectable signal (Figure 2A). We further investigated the binding specificity of RA16 using other cell lines, including NSCLC cell lines (NCI-H1299, SPC-A1, and NCI-H1650) as well as non-NSCLC cell lines (293T and HeLa). For NSCLC cells, RA16 showed strong binding to both NCI-H460 and NCI-H1299 cells, but weak binding (~5%) to NCI-H1650 cells as illustrated in Figure 2B by flow cytometry. The binding of RA16 toward SPC-A1 is minimal. In contrast to NSCLC cells, RA16 showed no binding to non-NSCLC 293T and HeLa cells. Moreover, no fluorescence was detected when HeLa cells and 293T cells were incubated with Cy3-labeled RA16 (Figure 2C). Notably, the labeling efficiencies of RA16 and RNA library by fluorescent dyes were comparable (Table S1), indicating the difference from labeling is neglectable.

*in vitro* selection may fail to perform favorably *in vivo*. Recent studies by Mi<sup>19</sup> and Cheng<sup>20</sup> identified RNA aptamers through *in vivo* evolution strategies, suggestive of the feasibility to screen the tumor-targeting aptamers within living animals.

In this study, we present a novel *in vivo* selection platform against NSCLC NCI-H460 tumor xenografted in nude mice. To improve the stability of the RNA pool for *in vivo* selection, we combined 2'-fluoropyrimidine modification together with polyethylene glycol (PEG, the process of PEGylation) before each selection round. After 11 selection rounds, an aptamer that specifically recognizes and inhibits NCI-H460 tumor was isolated. The aptamer was used as a carrier for targeted delivery of a chemotherapeutic, which enhanced the *in vitro* and *in vivo* cytotoxicity of the chemotherapeutic.

## RESULTS

### Direct *In Vivo* Selection of RNA Aptamer Using Xenograft Mouse Model

We hypothesized the tumor *in vivo* to be an optimal platform as compared with *in vitro* targets to screen and generate RNA aptamers against NSCLC. NCI-H460-bearing xenograft nude mouse model was established for the selection. We started with a previously reported DNA library containing 40 random nucleotides flanked by consensus sequences at both 5' and 3' ends.<sup>21</sup> The transcription of this DNA library can provide  $10^{14}$  to  $10^{15}$  unique RNA sequences, which were used for the selection process. To enhance the *in vivo* stability and circulatory half-life of RNA library in animals, 2'-fluoropyrimidines

**Table 1. Recovered Sequence from *In Vivo* Selection Platform**

DNA Library: CACTAATACGACTCACTATAGGGAGAGAACAATGACCTN(40)GAGTGCATTGCATCACGTCAGTAG		
RNA Pool	Top Five Sequences (40 nt Random Region, 5' → 3')	Frequency (%)
Round 8 (Sanger sequencing, 33 colonies)	<u>GCGGTGCCAAGCCGTCGGGTTATGTTGATCTCCTCAAGGAC</u>	21.2
	GACCGGAGGCCTAGCCAAACCGGACCGCTTAATGACTCTCA	6.1
	GTACTACCCACAAGAGGCTAGATACTAACTCTCCTACACC	3
	GATTGGCGCGAAATTCGGGCCACTCAAACAACCTCTGTGTAC	3
	GCGAACATATAATCGCAACAATGGCTGCAAGCTTAGCCAA	3
Round 11 (Sanger sequencing, 19 colonies)	<u>GCGGTGCCAAGCCGTCGGGTTATGTTGATCTCCTCAAGGAC</u>	94.7
	GACTCTGATGCCTCAGACATTGACGCTTCCTGCGCAAGTTG	5.3
RA16 ranked first after rounds 8 and 11 (underlined).		

These results demonstrate that RA16 is able to bind multiple NSCLC cell lines as an NSCLC-targeting aptamer.

We investigated the binding affinity of RA16 to NCI-H460 cells by determining the equilibrium dissociation constant ( $K_D$ ) using flow cytometry, the method widely used for characterizing the cell-SELEX aptamers.<sup>18,27</sup> Analysis of the fitted curve revealed a  $K_D$  value of  $9 \pm 2$  nM (Figure 2D) and was within the typical range displayed by aptamers,<sup>26,28</sup> showing the high affinity of RA16 to NCI-H460 cells.

#### Specificity of Selected the RNA Aptamer RA16 *In Vivo*

Having confirmed the specificity and high affinity of RA16 to NCI-H460 cells *in vitro*, we performed experiments to evaluate specificity of RA16 in the xenograft mouse. Cryosections from various organs of tumor-bearing mouse were collected and incubated with FITC-RA16 to verify tissue specificity *in vitro*. Strong binding of RA16 to NCI-H460 tumors was observed, with only weak signal detected with normal lung tissues. No significant binding was detected in other tissues from tumor-bearing mouse or control mouse (Figure 3A), demonstrating the high specificity of RA16 to NSCLC tumors. We confirmed the targeting activity of RA16 in living animals with qRT-PCR to trap specific RA16 from various tissues of tumor-bearing mouse. The selected RNA aptamer RA16, or initial RNA library was administrated and its distribution level determined by qRT-PCR. Mouse 18S RNA was used as a standard for normalization. As shown in Figure 3B, the RA16 level was significantly higher (10- to 100-fold) in NCI-H460 tumors as compared to any other organs including heart, liver, spleen, lung, and kidney. Moreover, a significant difference was observed in aptamer recovery level in the tumor. In mouse tumors, the trapped RA16 was  $44.3 \pm 3.6$ -fold higher than the trapped initial RNA library. No significant enrichment of RA16 was observed in tissues from control mice (Figure 3C), indicating the specific entrapment of RA16 in the tumor tissue *in vivo*.

We further performed an *in vivo* imaging assay to study RA16 binding in tumor-bearing mouse. The gradual movement of Cy5.5-labeled RA16 toward tumor sites was tracked. At 3.5 hr, RA16 was enriched at the tumor areas, as evident from the strong fluorescent signal at the tumor site. On the other hand, Cy5.5-labeled initial RNA library

was enriched at other sites and degraded with time (Figure 3D). These results show that RNA aptamer RA16 was specific against human NCI-H460 cells and xenograft tumor tissues and showed high affinity both *in vitro* and *in vivo*.

#### Anti-tumor Efficacy of the Selected RNA Aptamer RA16

Many aptamers are known to show inhibitory activities against their binding targets.<sup>29–31</sup> To evaluate the anti-cancer of RA16, NCI-H460 cells were incubated with RA16 or scramble RNA (sequence in Table S2) and the cell cytotoxicity determined after 48 hr. Aptamer RA16, but not scramble RNA control, inhibited cell proliferation by 75% at 300 nM concentration. Neither RA16 nor scramble RNA showed any inhibition on the proliferation of HeLa cells (Figure 4A). RA16 inhibited the cell growth of NCI-H460 in a dose-dependent manner. The inhibitory effect was observed from concentration of 10 nM, and its  $IC_{50}$  value was estimated to be  $\sim 116.7$  nM (Figures 4B and 4C). Under the same conditions, RA16 exhibited no inhibitory effect against HeLa cells even at 600 nM (data not shown).

We further investigated the inhibitory effect of RA16 against NCI-H460-bearing mouse. Tumor sizes were measured every other day and tumor volumes calculated. On day 6, a significant reduction in tumor growth was observed in mice treated with RA16 as compared to those in the control group, whereas the control scramble RNA did not show any inhibitory effect on tumor growth (Figure 4D). The average inhibition rate for tumors of RA16-treated group was  $54.26\% \pm 5.87\%$  compared with those of the control group (Table 2), indicating that RA16 was able to inhibit NCI-H460 tumor growth *in vivo*.

#### Formation of RA16-Epirubicin Adduct

Like Dox, epirubicin (EPI) is known to be widely used in chemotherapies against various cancers, including NSCLC.<sup>32–34</sup> It intercalates within double-stranded DNA strands through aromatic rings, in particular into double-stranded 5'-GC-3' or 5'-CG-3' sequences.<sup>35</sup> Studies have shown that EPI is also capable to intercalate into double-stranded GC pairs of RNA aptamers.<sup>36</sup> To explore the possibility of using the aptamer as a tumor-targeting carrier, we constructed an aptamer-EPI adduct for drug delivery studies. The two-dimensional structure of RA16 predicted by Mfold revealed eight possible sites

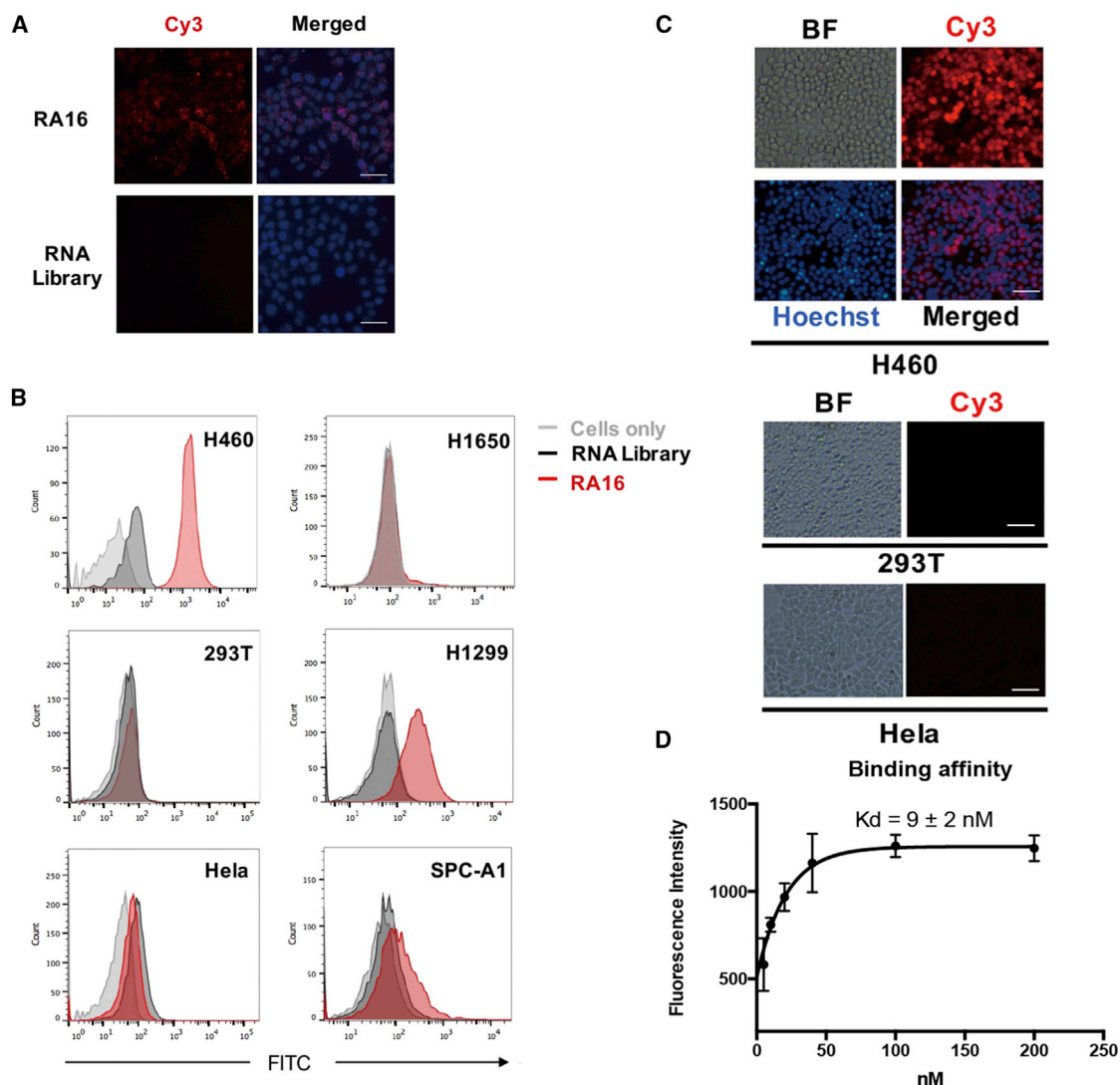


**Figure 2. Aptamer RA16 Demonstrates High Specificity to NCI-H460 Cell *In Vitro***

(A) Fluorescence microscopy revealed binding of RNA sequences to NCI-H460 cells. NCI-H460 cells were incubated with Cy3-labeled RNA molecules, and images were captured after 1 hr incubation (20 $\times$  objective; scale bar, 50  $\mu\text{m}$ ). (B) Flow cytometry to monitor aptamer binding to NSCLC cells and control cells. NCI-H460, HEK293T, HeLa, NCI-H1650, NCI-H1299, and SPC-A1 cells were incubated with FITC-labeled RNA molecules, and the fluorescence intensity was measured by flow cytometry. (C) Fluorescence microscopy revealed binding of aptamer RA16 to different cells. Images were captured after 1 hr incubation of cells with Cy3-labeled RA16 (10 $\times$  objective; scale bar, 100  $\mu\text{m}$ , BF represents images taken under bright field). (D) The binding curve of FITC-labeled RA16 (5–200 nM) and mean fluorescence intensities (MFIs) obtained by flow cytometry,  $K_D = 9 \pm 2 \text{ nM}$ . Three independent experiments were performed; all data represent means  $\pm$  SD,  $n = 3$ .

for EPI intercalation (Figure 5A). Indeed, the fluorescence exhibited by EPI is quenched after intercalation into the aptamer, similar to that observed with doxorubicin (DOX).<sup>36,37</sup> The formation of non-covalent adduct between RA16 and EPI was studied by measuring fluorescence. The fluorescence intensity was approximately 570 (a.u.) for free EPI; it decreased with the addition of increasing concentration of RA16. A steady minimum fluorescence was observed when the molar ratio of RA16 and EPI was 1:10 to 1:5 (Figure 5B). This observation is in agreement with the predicted eight intercalation sites, suggesting the non-covalent adduct of EPI to RA16 by interca-

lation into predicted double-stranded GC sequences. We also generated a scramble RNA that can presumably intercalate eight EPI molecules by forming RNA-EPI adduct as we measured through EPI fluorescence quenching (data not shown). We fixed the adduct molar ratio at 1:8 for subsequent *in vitro* and *in vivo* studies.

#### RA16-EPI Adduct Enhanced Specific Cytotoxicity against NCI-H460 *In Vitro*

Flow cytometry analysis was performed to assess the specificity of RA16-EPI adduct toward NCI-H460 cells. NCI-H460 cells exhibited

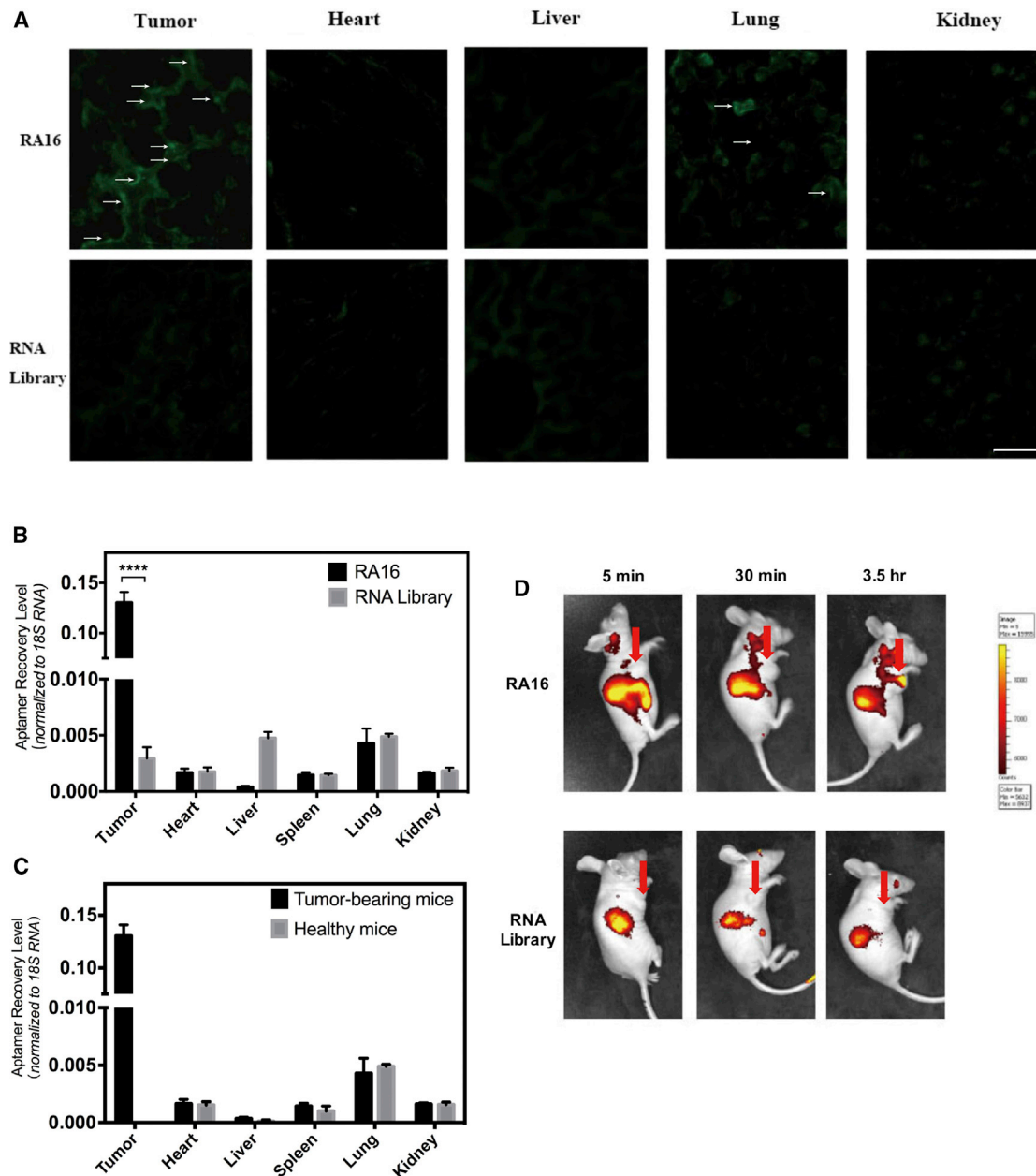


**Figure 3. Aptamer RA16 Shows Specificity to NCI-H460 Tumor *In Vivo***

(A) Cryosections from various organs of tumor-bearing mice were incubated with FITC-labeled RA16 or RNA library and photographed by microscope (10× objective; scale bar, 100 μm and applied to all images). (B) qRT-PCR was used to quantify RNA molecules in tumor, heart, liver, spleen, lung, and kidney. Mouse 18S RNA was used for normalization. All data represent means ± SD, n = 4. \*\*\*\*p < 0.0005. (C) qRT-PCR analysis of RA16 distribution in mice bearing NCI-H460 tumor (n = 4) and healthy mice (n = 4). All data represent means ± SD, with 18S RNA used as a loading control. The black bars in (B) and (C) are the same results repeated. (D) *In vivo* imaging of Cy5.5-labeled RNA molecules in mice bearing NCI-H460 tumor at different time points (0.5, 2, and 3.5 hr post-injection).

a fluorescence shift when incubated with RA16-EPI, as compared with those treated with scramble RNA-EPI, demonstrating that RA16-EPI retained specific binding to NCI-H460 cells (Figure 5C).

We evaluated the anti-cancer efficacy of the adduct *in vitro*. As shown in Figure 5D, RA16-EPI demonstrated significantly higher inhibitory

effects against NCI-H460 cells (Figure 5D). The inhibition rate was 85.20% ± 1.62% with RA16-EPI adduct as compared to 42.84% ± 1.67% and 54.86% ± 4.97% with free EPI (1.5 μM) and RA16 (0.1875 μM) alone, respectively, while scramble RNA-EPI exhibited an inhibition rate of 33.65% ± 5.14%, which was even less than the free EPI, presumably due to the capture of EPI by scramble RNA

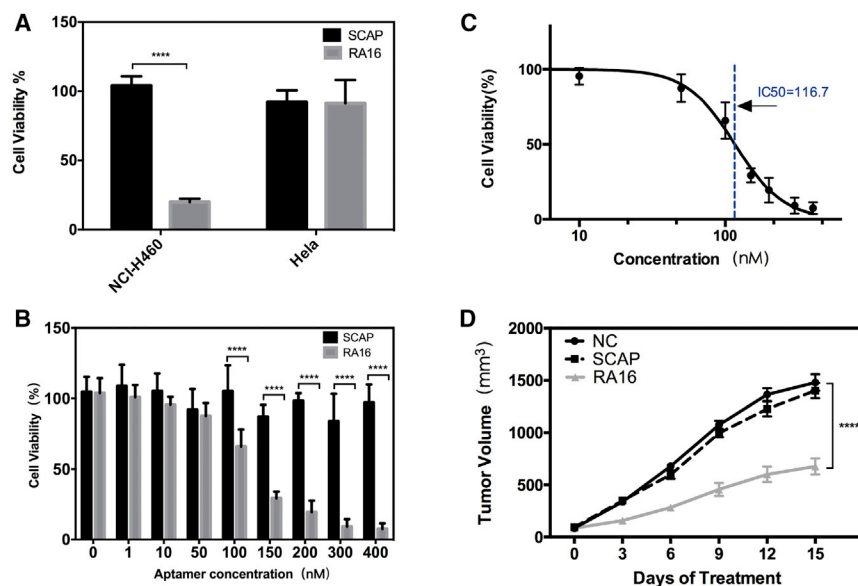


**Figure 4. APTAMER RA16 INHIBITS NCI-H460 CELL PROLIFERATION *In Vitro* AND *In Vivo***

(A) NCI-H460 and HeLa cells were evaluated with a standard CCK-8 assay after 48-hr incubation with 300 nM RA16 or scramble RNA. All data represent means  $\pm$  SD,  $n = 6$ . \*\*\*\* $p < 0.0005$ . (B) NCI-H460 cells were evaluated with a standard CCK-8 assay after 48-hr incubation with different doses of RA16 or scramble RNA. All data represent means  $\pm$  SD,  $n = 6$ . \*\*\*\* $p < 0.0005$ . (C)  $IC_{50}$  of RA16 to H460 cells. All data represent means  $\pm$  SD,  $n = 6$ . (D) Mice bearing NCI-H460 tumor were treated with saline, scramble RNA, or RA16. The length (L) and width (W) of tumors were determined every 3 days and the tumor volume (V) calculated using the formula  $V = 1/2 \times L \times W^2$ . Tumor growth was monitored from the start of the treatment. Results were expressed as mean tumor volume  $\pm$  SEM ( $n = 5$  per group, \*\*\*\* $p < 0.0005$ ).

lack of cell targeting. These results strongly indicate the additive anti-cancer efficacy by RA16-EPI adduct.

To assess the side toxicity of RA16-EPI, we studied cell viability in non-targeted tumor cell line (HeLa cells) treated with RA16-EPI adduct. We observed that both RA16-EPI and scramble RNA-EPI were less cytotoxic to HeLa cells and the inhibition rate recorded were  $71.91\% \pm 0.90\%$  and  $65.22\% \pm 3.43\%$ , respectively, compared to  $82.88\% \pm 0.90\%$  with free EPI (Figure 5E).

#### RA16-EPI Adduct Enhanced Anti-tumor Efficacy in Animal Model

To further evaluate efficacy of RA16-EPI adduct *in vivo*, first, we investigated the stability of RA16-EPI adduct and PEGylated RA16 in the serum *in vitro*. We first confirmed that during a 3 hr time period, the fluorescence intensity of free EPI degraded gradually; however, fluorescence of RA16-EPI adduct remained at a low level, indicating that EPI was intercalated into the RA16 structure in the presence of serum (Figure 6A). One critical question is whether the PEGylation of RA16 increases its *in vivo* stability. As illustrated in Figure 6B, more than 50% of PEGylated RA16 was still detected, whereas non-PEGylated RA16 disappeared almost completely after 1 hr incubation in 50% serum, demonstrating that PEGylated RA16 was more stable than non-PEGylated RA16 in serum.

Based on the higher stability of intercalated EPI and PEGylated RA16 in the serum, we further evaluated the anti-cancer efficacy of PEGylated RA16-EPI in xenograft tumor models. On day 9, a decrease in tumor growth was observed for mice treated with EPI alone, PEGylated RA16-EPI adduct, PEGylated scramble RNA-EPI adduct or RA16-EPI adduct without (w/o) PEGylation (Figure 6C). PEGylated-RA16 should have higher *in vivo* stability and longer circulatory half-life and thereby exhibit higher levels of tumor reduction

as compared to EPI alone, scramble RNA-EPI, or adduct w/o PEGylation (Figure 6C). On day 16, PEGylated RA16-EPI demonstrated a strong inhibition rate of  $64.38\% \pm 7.92\%$  as compared with the moderate inhibition observed with EPI alone ( $45.34\% \pm 10.83\%$ ), scramble RNA-EPI ( $36.83\% \pm 6.72\%$ ), or adduct w/o PEGylation ( $37.28\% \pm 9.14\%$ ) (Figures 6C and 6D; Table 2).

#### DISCUSSION

NSCLC is the leading cause of death from cancer all over the world.<sup>38</sup> Chemotherapies—conventional treatment strategies used to prolong survival of patients—display severe adverse effects.<sup>3,4</sup> RNA aptamers are considered as promising agents for targeted therapy, due to their high and specific target binding, small size, and low or non-immunogenicity. Over the years, aptamers with various potential applications against known targets such as vascular endothelial growth factor (VEGF), EGFR, mucin 1 (MUC1), and p53 have been developed.<sup>39–42</sup> Aptamers are typically obtained from *in vitro* selection against various targets, including proteins, small molecules, or whole cells. A few investigations are based on *in situ* screening system.

In this study, we demonstrated that highly specific aptamers can be developed by direct *in vivo* selection from a diverse, PEGylated RNA library against NSCLC NCI-H460-bearing mouse, and the resulting aptamer can be used for targeted delivery of a therapeutic agent.

This is the first study to combine post-selection modification with *in vivo* screening platform. The smaller size of aptamers makes them more susceptible to renal filtration as compared to higher molecular weight antibodies. It was reported that the clearance time of 2'-fluoro aptamer was 5~15 hr in plasma.<sup>21,43,44</sup> Studies have shown the use of PEG to counter immune responses and extend the circulatory half-life of proteins, peptides, or other molecules.<sup>45,46</sup> In addition, PEGylation may increase their persistence in the circulation.

**Table 2. Tumor Inhibition Rate**

Group	Inhibition of RA16			Inhibition of RA16-EPI Adduct				
	G1	G2	G3	G1	G2	G3	G4	G5
	Negative Control (Saline)	Scramble RNA	RA16	Negative Control (Saline)	EPI	Scramble RNA-EPI Adduct	RA16-EPI Adduct	Adduct w/o PEGylation
Tumor weight (g)	–	–	–	3.72 ± 0.67	2.03 ± 0.40	2.35 ± 0.25	1.33 ± 0.29	2.33 ± 0.34
Inhibition rate (%)	–	3.63	54.26	–	45.34 ± 10.82	36.83 ± 6.72	64.38 ± 7.92	37.27 ± 9.14

Inhibition rate (%) = (average tumor weight of control – average tumor weight of treated group)/average tumor weight of control × 100%.

Macugen, the only aptamer that received FDA approval<sup>40,47</sup> was introduced after PEGylation to overcome its rapid clearance and degradation *in vivo*. However, PEGylation may affect the structure and binding activity of the molecule *in vitro*.<sup>48,49</sup> In this study, we used PEGylated RNA sequences during *in vivo* SELEX to extend the half-life of the RNA pool, reducing renal clearance and simplifying the post-selection modification process. Our studies demonstrated that the enriched aptamer, RA16, still possesses targeting activity after fluorescently labeling, EPI intercalation, and PEGylated modification.

During the selection, the starting library, a mixture containing diverse structures of RNA molecules, was served as the control to monitor the enhanced targeting activity by the enriched aptamer. To further investigate the cytotoxicity and efficacy of the aptamer, scramble RNA was used as control, which is uniform and stable.

Given the extremely high complexity of *in vivo* environments and the large amount of repertoires exposed to the initial library, we performed several selection rounds *in vivo*. In contrast to the studies by Mi<sup>19</sup> and Cheng,<sup>20</sup> the enriched sequence RA16 emerged after eight rounds of selection and accounted for 90% the enriched RNA after round 11. Our efficient enrichment and *in vivo* SELEX process could be attributed to the following possibilities: (1) PEGylation enhanced the persistence of the RNA pool in the circulation, thereby increasing the chances of enrichment of the specific aptamer, or (2) long circulatory time eliminated non-specific binding. In order to maximize the PEGylation, T7 RNA polymerase should preferentially use guanosine monophosphate (GMP) to initiate RNA transcription *in vitro*, since all the reagents were excessive in the reaction.<sup>50</sup> Agarose gel results in Figure 1C demonstrated that more than 60%~70% of the RNA library was successfully PEGylated, indicating the high diversity of the PEGylated RNA library were achieved. It is crucial to pre-optimize the selection strategy. The selection efficiency can be further improved by optimizing parameters such as the number of mouse used in each round, the ratio of RNA pool versus mouse number, assessment criteria, and tumor size.

We explored the application of the best aptamer RA16 as a carrier for targeted delivery of chemotherapeutics. Given the intercalatable property of EPI into G-C pairs, it was used to bind RA16 and

form an aptamer-EPI adduct. Consistent with similar studies,<sup>15,27</sup> RA16-EPI adduct demonstrated specificity and improved cytotoxicity upon incubation with NCI-H460 cells. In addition, the adduct demonstrated enhanced anti-cancer efficacy when used for targeting tumors *in vivo*. The enhanced efficacy may be attributed to PEGylated RA16 that served as a carrier for the chemotherapeutic, resulting in higher retention of EPI at tumor sites than elsewhere. Moreover, it allowed gradual release of EPI, leading to improved cytotoxicity and enhanced efficacy. However, no significant difference in the inhibitory effect was observed between EPI alone or adduct without PEGylation. The aptamer without PEGylation as a non-covalent carrier of EPI may be unstable *in vivo*, leading to quick leakage and clearance of the cargo. Furthermore, the concentration of the aptamer used (approximately 325 pmol) may be insufficient to demonstrate tumor regression by aptamer. Tumor suppression by PEGylated RA16-EPI adduct was relatively stronger than that by adduct w/o PEGylation. Thus, PEGylation is important to maintain stable tertiary structure and prolong aptamer circulation time *in vivo*, which may result in the accumulation of anti-cancer agents at tumor site.

In conclusion, we present a novel study demonstrating that aptamers can be selected from tumors of living animals and that the combination of PEGylation with *in vivo* SELEX improves the selection efficiency as well as greatly facilitates the post-selection applications. The specificity, high affinity, and strong anti-cancer efficacy of the aptamer RA16 strongly suggest its potential application for targeted diagnostics. In addition, we derived RA16-chemo adduct and explored its tumor-targeting potential for clinical applications. We believe that further identification of potential targets of this aptamer on cancer cells could facilitate our understanding of molecular mechanisms of NSCLC.

## MATERIALS AND METHODS

### Cell Culture

NCI-H460, HEK293T, and other cell lines obtained from Cell Resource Center of Shanghai Institutes for Biological Sciences, CAS, were cultured in RPMI-1640 medium supplemented with 10% (v/v) fetal bovine serum (FBS), 100 U/mL penicillin, and 100 mg/mL streptomycin in an incubator (Thermo Fisher Scientific, USA) at 37°C, 5% CO<sub>2</sub>. Cells were sub-cultured approximately

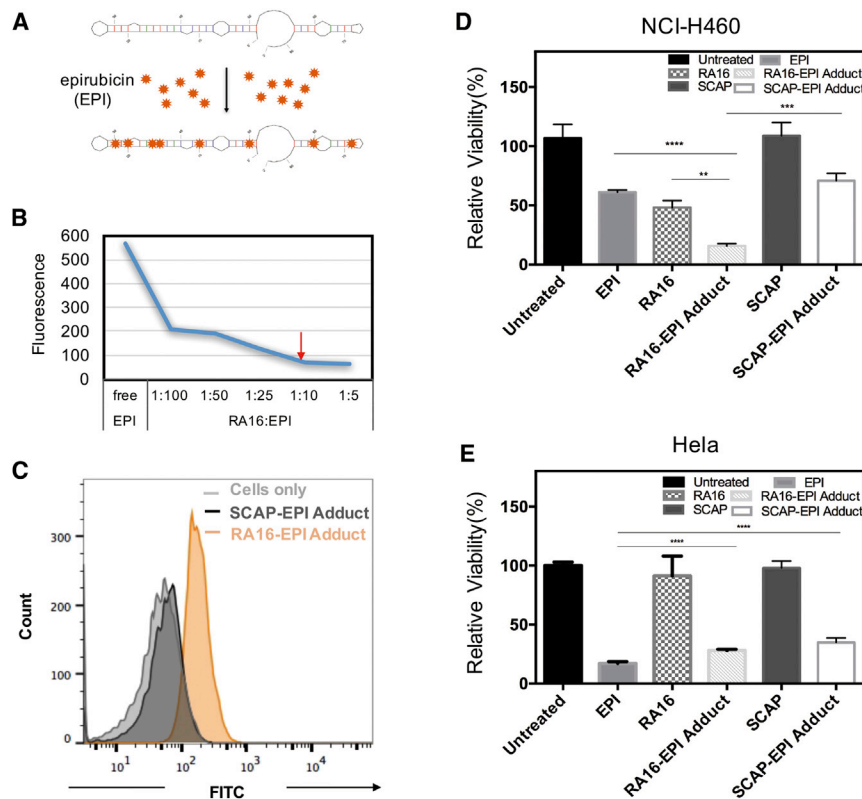


**Figure 5. Aptamer RA16-EPI Adduct Enhances Specific Cytotoxicity to NCI-H460 Cell**

(A) Schema of EPI intercalation. EPI can be intercalated non-covalently into base pairs, in particular, the GC pair. (B) Determination of fluorescence of EPI and RA16-EPI adduct. Different ratios of RA16 and EPI adduct were tested for EPI fluorescence. The fluorescence of the adduct was quenched due to EPI intercalation into aptamer ( $\lambda_{Ex} = 485$  nm,  $\lambda_{Em} = 580$  nm). (C) Flow cytometry to monitor aptamer-EPI adduct binding to NCI-H460 cells. NCI-H460 cells were incubated with FITC-labeled aptamer-EPI adduct and the fluorescence intensity detected by flow cytometry. (D and E) NCI-H460 (D) and HeLa (E) cells were evaluated with a standard CCK-8 assay after 48-hr incubation under the following treatment conditions: untreated, 1.5  $\mu$ M EPI, 187.5  $\mu$ M RA16, 187.5  $\mu$ M RA16-EPI adduct (RA16:EPI = 1:8), 187.5  $\mu$ M scramble RNA, and 187.5  $\mu$ M scramble RNA-EPI adduct (scramble RNA:EPI = 1:8). All data represent means  $\pm$  SD,  $n = 5$ . \*\*\*\* $p < 0.0005$ , \*\*\* $p < 0.001$ , \*\* $p < 0.01$ , analyzed by one-way ANOVA and Tukey's test for multiple comparisons.

pyrophosphatase (Thermo Fisher Scientific, USA). The resultant reaction was treated with 2  $\mu$ L DNase I (5 U/ $\mu$ L, RNase-free, TaKaRa, China) for 1 hr to eliminate template DNA. DNase I was inactivated with phenol-chloroform extraction. RNAs were then dissolved in 0.1 M sodium bicarbonate ( $\text{NaHCO}_3$  [pH 8.3]) and incubated with 30 kDa N-hydroxysuccinimide-PEG (NHS-PEG; PegBio, Jiangsu, China) for 2 hr at room temperature for PEG conjugation at the 5' end (Figure 1C).

Prior to SELEX, 2 nmol RNA library was further desalted with Amicon YM-10 columns (Merck Millipore, Germany) and dissolved in 300  $\mu$ L RNA refolding buffer (10 mM HEPES [pH 7.4], 50 mM NaCl, 1 mM  $\text{CaCl}_2$ , 1 mM  $\text{MgCl}_2$ , 2.7 mM KCl).<sup>13</sup> The solution was refolded by incubation on a heat block at 90°C for 3 min, followed by slow cooling to room temperature.

The RNA library was injected by tail vein in three mice bearing NCI-H460 tumor. After 6 hr, mice were sacrificed and tumors harvested. Tumors were rinsed with Dulbecco's phosphate-buffered saline (DPBS), and total RNAs extracted by TRIzol reagent, followed by treatment with RNase A and DNase I at 37°C for 30 min to recover RNAs from the initial RNA library.

To regenerate DNA template for the next round of selection, the enriched RNAs were reversely transcribed with M-MLV reverse transcriptase (RNase H<sup>-</sup>) (TaKaRa, China) followed by PCR amplification. The number of PCR cycles was optimized and the cDNA pool was amplified in a Taq PCR reaction containing 0.4  $\mu$ M each of 5' and 3' primers (Table S2), 1.5 mM  $\text{MgCl}_2$ , 80  $\mu$ M of each deoxynucleotide triphosphate (dNTP), and 0.05 U/ $\mu$ L Taq DNA polymerase (Sangon Technologies, Shanghai, China). cDNA was purified and

every 2 days at 80% confluence using 0.25% (w/v) trypsin at a split ratio of 1:3.

### Animals and Tumor Xenograft Models

All animal studies were performed in accordance with the Guide for Care and Use of Laboratory Animals, Soochow University (IACUC Permit Number SYXX [Su] 2013-0105). To establish tumor xenograft model, female BALB/c nude mice (5 weeks old, SLRC Laboratory Animal Center, Shanghai, China) were sub-cutaneously injected in the underarm with  $2 \times 10^6$  NCI-H460 cells. The tumor size was determined with a vernier calliper and the tumor volume (V) calculated as  $V = 1/2 \times L \times W^2$ , where L and W represent length and width of the tumor, respectively.

### In Vivo Selection

The starting RNA library containing 40 random nucleotides with  $\text{NH}_2$  at the 5' end was generated by *in vitro* transcription with mutant (Y639F) T7 RNA polymerase from a pre-constructed DNA library (Table 1) from the Liu lab at UNC at 37°C for 8 hr in the following transcription reaction: 10  $\times$  transcription buffer (400 mM Tris-Cl, 80 mM magnesium chloride [ $\text{MgCl}_2$ ], and 20 mM spermidine), 10 mM ATP, 10 mM guanosine triphosphate (GTP) (Sangon Technologies, Shanghai, China), 10 mM 2'-F-dCTP/dUTP, 5 mM aminally-GMP (TriLink Biotechnologies, CA, USA), 10 mM dithiothreitol (DTT), 20 U T7 (Y639F) RNA polymerase, 20 U RiboLock RNase Inhibitor (Thermo Fisher Scientific, USA), and 0.05 U inorganic

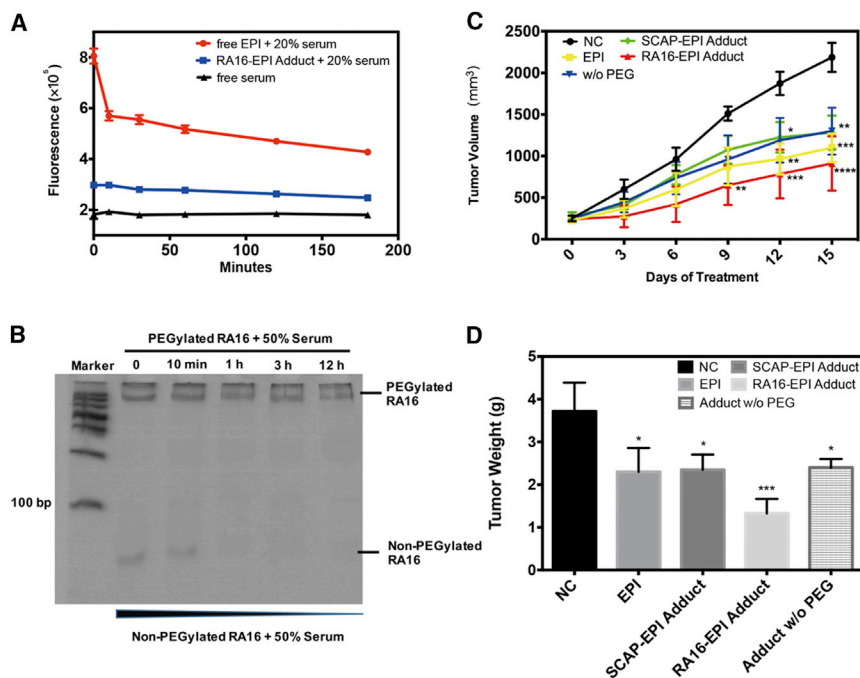


**Figure 6. RA16-EPI Adduct Enhances Cytotoxicity to NCI-H460 Xenograft Nude Mice**

(A) Stability of RA16-EPI adduct in the serum. Free EPI, RA16-EPI adduct, and serum were quantified by EPI fluorescence in the 20% serum. The fluorescence of EPI decreased with time, while that of RA16-EPI adduct remained quenched due to EPI intercalation ( $\lambda_{Ex} = 485 \text{ nm}$ ,  $\lambda_{Em} = 595 \text{ nm}$ ). (B) Stability of PEGylated RA16 in the serum. PEGylated or non-PEGylated RA16 was incubated with 50% serum, and survival of RNA molecules were monitored by 12% native-PAGE gel. (C) Mice bearing NCI-H460 tumor were treated with saline, EPI alone, scramble RNA-EPI adduct, RA16-EPI adduct, or adduct without PEG, and the length (L) and width (W) of the tumor determined every 3 days as follows:  $V = 1/2 \times L \times W^2$ . Tumor growth was monitored from the start of the treatment. Results were expressed as mean tumor volumes  $\pm$  SEM ( $n = 5$  per group, \*\*\*\* $p < 0.0005$ , \*\*\* $p < 0.001$ , \*\* $p < 0.01$ , \* $p < 0.05$ ), analyzed by two-way ANOVA followed by Tukey's test for multiple comparisons to saline. (D) Tumor weight was determined when mice were sacrificed at day 16 ( $n = 3-5$  per group, \*\*\*\* $p < 0.001$ , \* $p < 0.05$ ).

recycled by MiniBEST Agarose Gel DNA Extraction Kit (TaKaRa, China). Purified and amplified double-stranded DNA (dsDNA) pool was *in vitro* transcribed into RNA pool followed by PEGylation for the next round of selection, as described above.

After every three rounds of selection, recovered cDNAs were cloned into T-vector (TaKaRa, China) following the manufacturer's protocol and sequenced by Sangon Technologies (Shanghai, China).

#### Fluorescent Labeling of RNA Aptamers

DNA templates of aptamers were *in vitro* transcribed into RNA by mutant T7 RNA polymerase and incorporated with aminoallyl-GMP (TriLink Biotechnologies, USA) to replace the 5' end of GTP. After transcription, the reaction mixture was treated with 2  $\mu\text{L}$  DNase I (5 U/ $\mu\text{L}$ , RNase-free) for 1 hr to eliminate the template DNA, followed by phenol-chloroform extraction to deactivate DNase I. To generate fluorescein-containing aptamers, RNA pellets were suspended in 0.1 M  $\text{NaHCO}_3$  (pH 8.3) and incubated with NHS-Cy3 (GE Healthcare, MA, USA), fluorescein isothiocyanate (FITC) (Life Technologies, USA) or NHS-Cy5.5 (GE Healthcare, MA, USA). Excess of fluorescent dye was neutralized with 10 mM Tris, and the solution was filtered using Amicon YM-10 filter to generate fluorescently labeled RNA transcripts. The absorption of the fluorescent dyes and RNAs were detected by One Drop to monitor the labeling efficiency.

#### Fluorescence Microscopy

NCI-H460, HeLa, and other cell lines were grown to 70% confluence on coverslips. These coverslips and mouse tissue cryosections were incubated with 200 nM fluorescent-labeled aptamer in HEPES-buff-

ered saline (HBS) containing 1.0  $\mu\text{g}/\text{mL}$  tRNA for 1 hr at 37°C. Cells were fixed with 4% paraformaldehyde for 10 min and washed thrice with DPBS. The nucleus was stained with Hoechst33342 (Thermo Fisher Scientific, USA) and cells imaged under a microscope (Olympus, Tokyo, Japan).

#### Flow Cytometry

NSCLC cells, HEK293T, and HeLa cells were grown to 70% confluence in 24-well plates, washed with HBS (RNA refolding buffer containing 1% BSA), and incubated with FITC-labeled aptamer in serum-free medium at 37°C for 2 hr. Cells were washed twice with DPBS and suspended in fluorescence-activated cell sorting (FACS) buffer (BD Bioscience, USA). Flow cytometry data were obtained using FACSVerser system (Becton Dickinson, NJ, USA), with 10,000 event acquisition for each sample and analyzed using FlowJo software (version X 10.0, <https://www.flowjo.com/>).

#### Fluorescence-Based $K_D$ Determination

Cells were treated as above and incubated with series concentrations (0 to 200 nM) of FITC-labeled aptamer for FACS analysis. The mean fluorescence intensity (MFI) of samples was obtained to calculate the  $K_D$  value for the interaction between RA16 and NCI-H460 cell using the equation  $F = B_{\max} \times [L]/(K_D + [L])$ , where F = fluorescence intensity and [L] = concentration of FITC-RA16.<sup>18,27</sup>

#### qRT-PCR for *In Vivo* Trap Assay

Four mice were administered RA16 at 500 pmol concentration via tail vein. After 3.5 hr, RNAs were extracted from tumor, heart, liver, lung, spleen, and kidney using TRIzol reagent following the manufacturer's protocol. The amount of RNA was quantified (One Drop), and 500 ng

DNase I-treated RNAs were used for reverse transcription using M-MLV transcriptase (TaKaRa, China). The relative abundance of RNA was quantified using qRT-PCR with appropriate primers and Power SYBR Green Master Mix (Life Technologies, USA) with StepOne Plus Real-Time PCR system (Applied Biosystems, USA). Mouse 18S RNA (primer sets from Sangon Technologies) was used for normalization.

#### **In Vivo Imaging Study**

Mice bearing NCI-H460 tumor were used for *in vivo* imaging assay. When the tumors size reached 200–300 mm<sup>3</sup>, mice were injected with Cy5.5-labeled aptamer at 1 nmol concentration via tail vein. Images were taken on IVIS Lumina Imaging system II (PerkinElmer, USA) at 0.5, 2, and 3.5 hr post-injection.

#### **In Vitro Cytotoxicity**

NCI-H460 and other cells ( $2 \times 10^4$  cells per well) were seeded in 96-well plates. After 24 hr incubation, cells were treated with RA16 or scrambled aptamer (sequence in Table S2) added in fresh medium at different concentrations. Following incubation for 48 hr, cell viability was determined as per the Cell Counting Kit-8 (CCK-8) protocol (Dojindo, Tokyo, Japan). Absorbance was measured at 450-nm wavelength using a microplate reader (Thermo Fisher Scientific, USA).

#### **In Vivo Anti-tumor Efficacy**

Mice bearing NCI-H460 tumor were weighed and randomly divided into different groups when tumors reached a size of 50–100 mm<sup>3</sup>. The RNA molecules for treatment were generated by *in vitro* transcription with mutant (Y639F) T7 RNA polymerase from the DNA template as described above. Mice were administrated saline (control), 2 nmol scramble RNA or RA16 via intravenous injection on days 0, 3, 5, 7, and 9. Tumor size was measured every other day and tumor volume calculated as described above. At day 16, mice were sacrificed, tumors and other organs were collected and weighed, and the inhibition rate was measured.

#### **Aptamer-EPI Adduct Formation**

For non-covalent adduct of the aptamer to EPI, RA16 or scramble RNA was first dissolved in RNA refolding buffer, followed by 3-min incubation on a heat block at 90°C. The reaction mixture was slowly cooled to room temperature to form a uniform secondary structure. The aptamer was added into an EPI solution at various concentrations to obtain EPI/aptamer molar ratios of 100, 50, 25, 10, and 5. After 2 hr incubation, fluorescence of EPI was measured in a 96-well black plate using Synergy Neo Analyzer (excitation wavelength = 485 nm, emission wavelength = 580 nm, BioTek, USA). The adduct was freshly prepared before each experiment. For adduct, the molar ratio of RA16/scramble RNA and EPI was fixed at 1:8.

#### **Cell Viability Evaluation**

NCI-H460 and HeLa cells ( $2 \times 10^4$  cells per well) were cultured in 96-well plates for 24 hr. Cells were treated with 1.5 μM EPI, 187.5 nM RA16, scramble RNA, RA16-EPI adduct, and scramble RNA-EPI adduct for 48 hr, followed by CCK-8 determination as

described by the manufacturer's protocol. Absorbance was measured at 450 nm wavelength with a microplate reader (Thermo Fisher Scientific, USA).

#### **Serum Stability of RA16-EPI Adduct**

To monitor the stability of RA16-EPI adduct in the serum, 3 μM EPI, 375 nM RA16-EPI, and vehicle control were incubated with 20% serum free of chelating agents. Fluorescence of free EPI was measured in a 96-well black plate by FilterMax F5 Multi-Mode Reader (excitation wavelength = 485 nm, emission wavelength = 595 nm, Molecular Devices, Austria). The adduct was freshly prepared for each experiment.

#### **Serum Stability of PEGylated RA16**

Five picomoles of PEGylated RA16 and non-PEGylated RA16 mixture was incubated in 50% serum without chelating agents, for 0 min, 10 min, 1 hr, 3 hr, and 12 hr, respectively. RA16 samples after incubation were then loaded onto a 12% native PAGE gel, followed by GelRed (Solarbio, Beijing, China) staining for visualization and quantification.

#### **In Vivo Efficacy of RA16-EPI Adduct**

Mice bearing NCI-H460 tumor were weighed and randomly divided into different groups after the tumor size reached 200–300 mm<sup>3</sup>. Mice (n = 5) from each group received either saline (control), free EPI (1.5 mg/kg), PEGylated RA16-EPI, PEGylated scramble RNA-EPI, or RA16-EPI w/o PEGylation (EPI at 1.5 mg/kg) weekly. Tumor size was measured every other day and tumor volume determined as described above. On day 16, mice were sacrificed, tumors and other organs were excised and weighed, and inhibition rate was monitored.

#### **Statistical Analysis**

Each experiment was repeated at least thrice with duplication for each sample tested. Results are presented as means ± SD, unless otherwise indicated. Statistical analysis and graphs were generated by GraphPad PRISM (version 6, GraphPad, CA, USA). Statistical differences were evaluated using one-way ANOVA, unless otherwise indicated. A value of  $p < 0.05$  was considered statistically significant.

#### **SUPPLEMENTAL INFORMATION**

Supplemental Information includes two tables and can be found with this article online at <https://doi.org/10.1016/j.omtn.2017.12.003>.

#### **AUTHOR CONTRIBUTIONS**

H.W., Y.Z., X.D., R.L., and Y.J. were involved in the design of the study. H.W. and Y.Z. performed the experiments. H.W., H.Y., and M.Q. performed the data analysis and interpretation. H.W., R.L., and Y.J. wrote the manuscript.

#### **CONFLICTS OF INTEREST**

Y.Z., H.Y., and M.Q. are employees of Biopharmagen Corp. The other authors declare no conflicts of interest.

## ACKNOWLEDGMENTS

This work is supported by funds from the State New Drug Research & Development, China (2011ZX09401-027). We thank Soochow University for mouse care and use administration. We also thank Dr. Irvin S.Y. Chen and Dr. Masakazu Kamata from University of California, Los Angeles for their insightful suggestions.

## REFERENCES

1. Visbal, A.L., Leigh, N.B., Feld, R., and Shepherd, F.A. (2005). Adjuvant chemotherapy for early-stage non-small cell lung cancer. *Chest* 128, 2933–2943.
2. NSCLC Meta-Analyses Collaborative Group (2008). Chemotherapy in addition to supportive care improves survival in advanced non-small-cell lung cancer: a systematic review and meta-analysis of individual patient data from 16 randomized controlled trials. *J. Clin. Oncol.* 26, 4617–4625.
3. Ruiz-Ceja, K.A., and Chirino, Y.I. (2017). Current FDA-approved treatments for non-small cell lung cancer and potential biomarkers for its detection. *Biomed. Pharmacother.* 90, 24–37.
4. Sabari, J.K., Santini, F., Bergagnini, I., Lai, W.V., Arbour, K.C., and Drilon, A. (2017). Changing the therapeutic landscape in non-small cell lung cancers: the evolution of comprehensive molecular profiling improves access to therapy. *Curr. Oncol. Rep.* 19, 24.
5. Melosky, B. (2017). Current treatment algorithms for patients with metastatic non-small cell, non-squamous lung cancer. *Front. Oncol.* 7, 38.
6. Liu, T.C., Jin, X., Wang, Y., and Wang, K. (2017). Role of epidermal growth factor receptor in lung cancer and targeted therapies. *Am. J. Cancer Res.* 7, 187–202.
7. Thakur, M.K., and Wozniak, A.J. (2017). Spotlight on necitumumab in the treatment of non-small-cell lung carcinoma. *Lung Cancer (Auckl.)* 8, 13–19.
8. Tuerk, C., and Gold, L. (1990). Systematic evolution of ligands by exponential enrichment: RNA ligands to bacteriophage T4 DNA polymerase. *Science* 249, 505–510.
9. Ellington, A.D., and Szostak, J.W. (1990). In vitro selection of RNA molecules that bind specific ligands. *Nature* 346, 818–822.
10. Bunka, D.H., and Stockley, P.G. (2006). Aptamers come of age—at last. *Nat. Rev. Microbiol.* 4, 588–596.
11. Sridharan, K., and Gogtay, N.J. (2016). Therapeutic nucleic acids: current clinical status. *Br. J. Clin. Pharmacol.* 82, 659–672.
12. Fang, X., and Tan, W. (2010). Aptamers generated from cell-SELEX for molecular medicine: a chemical biology approach. *Acc. Chem. Res.* 43, 48–57.
13. Zhou, J., Li, H., Zhang, J., Piot, S., and Rossi, J. (2011). Development of cell-type specific anti-HIV gp120 aptamers for siRNA delivery. *J. Vis. Exp.* 2011, 2954.
14. Mayer, G. (2009). The chemical biology of aptamers. *Angew. Chem. Int. Ed. Engl.* 48, 2672–2689.
15. Xiang, D., Shigdar, S., Qiao, G., Wang, T., Kouzani, A.Z., Zhou, S.F., Kong, L., Li, Y., Pu, C., and Duan, W. (2015). Nucleic acid aptamer-guided cancer therapeutics and diagnostics: the next generation of cancer medicine. *Theranostics* 5, 23–42.
16. Mor-Vaknin, N., Saha, A., Legendre, M., Carmona-Rivera, C., Amin, M.A., Rabquer, B.J., Gonzales-Hernandez, M.J., Jorns, J., Mohan, S., Yalavarthi, S., et al. (2017). DEK-targeting DNA aptamers as therapeutics for inflammatory arthritis. *Nat. Commun.* 8, 14252.
17. Yoon, S., Huang, K.W., Reebye, V., Spalding, D., Przytycka, T.M., Wang, Y., Swiderski, P., Li, L., Armstrong, B., Reccia, I., et al. (2017). Aptamer-drug conjugates of active metabolites of nucleoside analogs and cytotoxic agents inhibit pancreatic tumor cell growth. *Mol. Ther. Nucleic Acids* 6, 80–88.
18. Shangguan, D., Li, Y., Tang, Z., Cao, Z.C., Chen, H.W., Mallikaratchy, P., Sefah, K., Yang, C.J., and Tan, W. (2006). Aptamers evolved from live cells as effective molecular probes for cancer study. *Proc. Natl. Acad. Sci. USA* 103, 11838–11843.
19. Mi, J., Liu, Y., Rabbani, Z.N., Yang, Z., Urban, J.H., Sullenger, B.A., and Clary, B.M. (2010). In vivo selection of tumor-targeting RNA motifs. *Nat. Chem. Biol.* 6, 22–24.
20. Cheng, C., Chen, Y.H., Lennox, K.A., Behlke, M.A., and Davidson, B.L. (2013). In vivo SELEX for identification of brain-penetrating aptamers. *Mol. Ther. Nucleic Acids* 2, e67.
21. Friedman, A.D., Kim, D., and Liu, R. (2015). Highly stable aptamers selected from a 2'-fully modified fGmH RNA library for targeting biomaterials. *Biomaterials* 36, 110–123.
22. Keefe, A.D., and Cload, S.T. (2008). SELEX with modified nucleotides. *Curr. Opin. Chem. Biol.* 12, 448–456.
23. Zuker, M. (2003). Mfold web server for nucleic acid folding and hybridization prediction. *Nucleic Acids Res.* 31, 3406–3415.
24. Shi, H., Cui, W., He, X., Guo, Q., Wang, K., Ye, X., and Tang, J. (2013). Whole cell-SELEX aptamers for highly specific fluorescence molecular imaging of carcinomas in vivo. *PLoS ONE* 8, e70476.
25. Shi, H., Tang, Z., Kim, Y., Nie, H., Huang, Y.F., He, X., Deng, K., Wang, K., and Tan, W. (2010). In vivo fluorescence imaging of tumors using molecular aptamers generated by cell-SELEX. *Chem. Asian J.* 5, 2209–2213.
26. Tang, Z., Shangguan, D., Wang, K., Shi, H., Sefah, K., Mallikaratchy, P., Chen, H.W., Li, Y., and Tan, W. (2007). Selection of aptamers for molecular recognition and characterization of cancer cells. *Anal. Chem.* 79, 4900–4907.
27. Hu, Y., Duan, J., Zhan, Q., Wang, F., Lu, X., and Yang, X.D. (2012). Novel MUC1 aptamer selectively delivers cytotoxic agent to cancer cells in vitro. *PLoS ONE* 7, e31970.
28. Shangguan, D., Meng, L., Cao, Z.C., Xiao, Z., Fang, X., Li, Y., Cardona, D., Witek, R.P., Liu, C., and Tan, W. (2008). Identification of liver cancer-specific aptamers using whole live cells. *Anal. Chem.* 80, 721–728.
29. Chen, Y., and Lin, J.S. (2017). The application of aptamer in apoptosis. *Biochimie* 132, 1–8.
30. Missailidis, S., and Hardy, A. (2009). Aptamers as inhibitors of target proteins. *Expert Opin. Ther. Pat.* 19, 1073–1082.
31. Li, N., Nguyen, H.H., Byrom, M., and Ellington, A.D. (2011). Inhibition of cell proliferation by an anti-EGFR aptamer. *PLoS ONE* 6, e20299.
32. Guaraldi, M., Marino, A., Pannuti, F., Farabegoli, G., and Martoni, A. (2001). Phase II study of sequential treatment of advanced non-small-cell lung cancer: three cycles of high-dose epirubicin plus cisplatin followed by weekly vinorelbine. *Clin. Lung Cancer* 3, 43–46, discussion 47–48.
33. Van Putten, J.W. (2001). Activity of the combination of high-dose epirubicin with gemcitabine in advanced non-small-cell lung cancer. *Lung Cancer* 34 (Suppl 4), S61–S64.
34. Wachters, F.M., Van Putten, J.W., Kramer, H., Erjavec, Z., Eppinga, P., Strijbos, J.H., de Leede, G.P., Boezen, H.M., de Vries, E.G., and Groen, H.J. (2003). First-line gemcitabine with cisplatin or epirubicin in advanced non-small-cell lung cancer: a phase III trial. *Br. J. Cancer* 89, 1192–1199.
35. Chaires, J.B., Herrera, J.E., and Waring, M.J. (1990). Preferential binding of daunomycin to 5'ATCG and 5'ATGC sequences revealed by footprinting titration experiments. *Biochemistry* 29, 6145–6153.
36. Haj, H.T., Salerno, M., Priebe, W., Kozlowski, H., and Garnier-Suillerot, A. (2003). New findings in the study on the intercalation of bisdaunorubicin and its monomeric analogues with naked and nucleus DNA. *Chem. Biol. Interact.* 145, 349–358.
37. Bagalkot, V., Farokhzad, O.C., Langer, R., and Jon, S. (2006). An aptamer-doxorubicin physical conjugate as a novel targeted drug-delivery platform. *Angew. Chem. Int. Ed. Engl.* 45, 8149–8152.
38. Torre, L.A., Bray, F., Siegel, R.L., Ferlay, J., Lortet-Tieulent, J., and Jemal, A. (2015). Global cancer statistics, 2012. *CA Cancer J. Clin.* 65, 87–108.
39. Bates, P.J., Laber, D.A., Miller, D.M., Thomas, S.D., and Trent, J.O. (2009). Discovery and development of the G-rich oligonucleotide AS1411 as a novel treatment for cancer. *Exp. Mol. Pathol.* 86, 151–164.
40. Ng, E.W., Shima, D.T., Calias, P., Cunningham, E.T., Jr., Guyer, D.R., and Adamis, A.P. (2006). Pegaptanib, a targeted anti-VEGF aptamer for ocular vascular disease. *Nat. Rev. Drug Discov.* 5, 123–132.
41. Ferreira, C.S.M., Papamichael, K., Guilbault, G., Schwarzacher, T., Garipey, J., and Missailidis, S. (2008). DNA aptamers against the MUC1 tumour marker: design of

- aptamer-antibody sandwich ELISA for the early diagnosis of epithelial tumours. *Anal. Bioanal. Chem.* *390*, 1039–1050.
42. Chen, L., Rashid, F., Shah, A., Awan, H.M., Wu, M., Liu, A., Wang, J., Zhu, T., Luo, Z., and Shan, G. (2015). The isolation of an RNA aptamer targeting to p53 protein with single amino acid mutation. *Proc. Natl. Acad. Sci. USA* *112*, 10002–10007.
43. Pieken, W.A., Olsen, D.B., Benseler, F., Aurup, H., and Eckstein, F. (1991). Kinetic characterization of ribonuclease-resistant 2'-modified hammerhead ribozymes. *Science* *253*, 314–317.
44. Burmeister, P.E., Lewis, S.D., Silva, R.F., Preiss, J.R., Horwitz, L.R., Pendergrast, P.S., McCauley, T.G., Kurz, J.C., Epstein, D.M., Wilson, C., and Keefe, A.D. (2005). Direct in vitro selection of a 2'-O-methyl aptamer to VEGF. *Chem. Biol.* *12*, 25–33.
45. Fishburn, C.S. (2008). The pharmacology of PEGylation: balancing PD with PK to generate novel therapeutics. *J. Pharm. Sci.* *97*, 4167–4183.
46. Harris, J.M., and Chess, R.B. (2003). Effect of pegylation on pharmaceuticals. *Nat. Rev. Drug Discov.* *2*, 214–221.
47. Bouchard, P.R., Hutabarat, R.M., and Thompson, K.M. (2010). Discovery and development of therapeutic aptamers. *Annu. Rev. Pharmacol. Toxicol.* *50*, 237–257.
48. Zhang, X., Wang, H., Ma, Z., and Wu, B. (2014). Effects of pharmaceutical PEGylation on drug metabolism and its clinical concerns. *Expert Opin. Drug Metab. Toxicol.* *10*, 1691–1702.
49. Foster, G.R. (2010). Pegylated interferons for the treatment of chronic hepatitis C: pharmacological and clinical differences between peginterferon-alpha-2a and peginterferon-alpha-2b. *Drugs* *70*, 147–165.
50. Kuzmine, I., Gottlieb, P.A., and Martin, C.T. (2003). Binding of the priming nucleotide in the initiation of transcription by T7 RNA polymerase. *J. Biol. Chem.* *278*, 2819–2823.